Analysis of a Unibody Stub Axle-Hub Design for an ATV

Urooj Ahmad, Subrath Praharaj
Department of Mechanical Engineering, BITS Pilani, Hyderabad Campus

Abstract

The aim of this paper is to design a unibody hub and stub axle Wheel assembly. For any ground vehicle, its dynamics and control behavior are majorly governed by the design of this assembly since it experiences all the major loads the vehicle faces. Our aim was to design and fabricate a unibody hub and stub axle which is light weight and more durable in comparison to the present form of design in which hub and stub axle is manufactured and assembled separately. Advantages of this unibody design is lesser components, easy replacement and easy manufacturing. This report also considers simulation of this unibody using FEM through Ansys, considering all the forces acting on the unibody. Also cost and strength comparison of different materials is done for selection of the best material. Design is done in such a way so as to consider all the parameters including performance, reliability, manufacturability, serviceability, weight and cost. Through this technique, the total unsprung mass of a vehicle is decreased by a major extent and the dynamic performance of the vehicle is also increased due to this without any change to suspension geometry or any other parts of the car.

Introduction

The Wheel Hub is an automobile part used inside most ground vehicles. It is an arrangement setup involving wheel, knuckles and brakes; it contains knuckle bearing and it holds the steering/suspension knuckle/upright and brake rotor. The wheel rims are bolted to the wheel Hub. The function of the component is to let the wheel spin unrestrained on the bearing keeping it attached to the automobile. This hub itself is the component which keeps the wheels attached to the automobile. In a ground auto-mobile suspension setup, the un-sprung mass of a vehicle is not supported by the suspension system. It involves masses of components in the likes of bearings, tires, wheel hubs, axles, and weight component of the shocks, driveshaft and control arms or links. In case of outboard braking, it is also considered under unsprung mass. The unsprung mass provides an alternative between a wheel's reactivity to the bump reaction and its modal decoupling. Surface irregularities on the road induce a load on this mass. The mentioned mass then has motion reaction to the loads generated due the bumps. This reaction amplitude for impulse-based bumps has an inverse relation to this weight. A lighter wheel will have more traction when it travels on an irregularly surfaced road. This is the main rationale for the objective behind choosing lighter wheels for high performance vehicles. Greater unsprung mass also worsens vehicle control due to increased slipping under hard throttling or hard braking. If the wheel positioning for the automobile on the vertical plane is not optimized, the loads exerted by hard throttling or braking in combination with higher un-sprung weight can lead to extreme cases of wheel hop.
Thus compromising handling of the vehicle.

An extensive research was performed on different optimization techniques used for redesign and evaluation of mechanical components. Karen and Ozturk [1] presented a paper describing a redesign of a failed clutch fork using topological optimization algorithms. The stress life approach was followed to establish a relation between fault position on the component which underwent failure and the numerical method of the simulation. The mass was reduced by nearly 24%, maximum stress was reduced by 9% and rigidness increased up to 40% with respect to the original component. S. Dhar [2] performed fatigue and crack propagation analysis on a wheel hub manufactured using material, pressure die Aluminum. He reports a corner crack reported a total failure in the component rendering it unusable. Instead of numerically analyzing the cause of failure, analytical tools were used, mainly linear elastic fracture mechanics. The nonlinear behavior was attributed to the structural discontinuities and heterogeneities. The analytical estimation also gave solution to the life of the component in service. The topology and heterogeneity of a fracture/crack/fault surface make the process of analyzing a crack growth initializing extremely complex. Fractal analysis and metallurgical studies aid in understanding the fracture problem.

The novelty and motivation of this study is the need to provide viable solutions to the problem of increased unsprung mass commonly encountered in ATVs. Given the light weighted nature of the vehicle an increased unsprung mass is detrimental to the Driver Handling as well as space optimization for other subsystems. This design aims to overcome these issues. We start by discussing the methodology and considerations for material and design selection. We approach this using a product design approach to understand it marketing viability. We then do a detailed analysis on possible forces experienced by the carrier assembly. In a lot of literature pertaining to ATV wheel carriers we found a lack of rigorous analysis on this part with some important contributing loads missing in the analysis [8] [9] [10] [11] [12]. We then include a DFMEA study to maintain our Product Design approach on safety analysis, highlighting the severity of failure in the component and justifying our choice of FOS. Finally, we do a detailed analysis of the CAD design and run an iterative optimization solver constraining Mass and FOS to obtain our final product. Both Static and Dynamic Analysis have been done and appropriate tools such as Biaxiality indication have been used to analyse and arrive at an acceptable solution.

Design Consideration

Wheel hub is a high safety component that should not yield to the generated Forces. The primary outliers for the modelling of the wheel hub assembly are:

- Forces acting on the assembly
- The process of manufacturing
- Behaviour of the Materials used

The effects of the above outliers are correlated, thus material behaviour under the loads will change in accordance with the design and the forces. The vehicle constraints must be kept in mind and the most economical alternative in coherence with optimal performance results, must be chosen. For this, we defined a new quantity, the cost per unit yield strength of the materials considered, we define this as C,

$$C = c_m * (\text{Density of Material}) / (\text{Yield Strength})$$

Where, c_m is the cost per unit mass of material. The following plot gives us an idea about the material to be chosen:

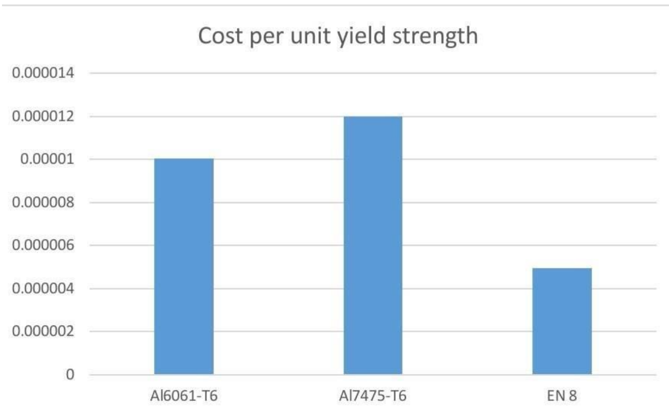

Figure 1. Cost per unit strength plot of 3 materials, 2 Aluminum variants and 1 steel variant.

But there are 2 other factors to be considered keeping in mind the unibody design. Machinability and Weight. Here Aluminum 6061-T6 beats EN 8 taking a lesser weight for the design and proving to be easily machinable owing to lesser Brinell hardness. [13][14]

Force Analysis

The data for the analysis has been taken from standard observed values from testing and performance of a BAJA ATV. [19][20]

$F_{STEP} = 300$ N ~ 30 KgF; PR = 6:1

$$F_{MC} = PR * F_{STEP} = 1800 \text{ N} \quad (1)$$

From Pascal's Law,

$$F_{PISTON} = 1800 \text{ N} * (D_{PISTON,\ C} * D_{PISTON,\ MC})^2 = 4449.98\text{N} \quad (2)$$

$$T_{BRAKING} = F_{PISTON} * \mu_{PAD} * N_{PISTON} * D_{RIM} * f_{REAR} = 395.16 \text{ Nm} \quad (3)$$

Considering a bump force of 3G as upper limit for Higher FOS,
$V_{MAX} = 57.16$ Km/h; $M_{VEHICLE} = 300$ Kg

$$F_{BUMP} = M_{VEHICLE} * 3 * 9.8 * f_{REAR} / 2 = 2646\text{N} \quad (4)$$

Thus, 661.5 N on Each petal.

$$F_{CORNERING} = f_{REAR} / 2 * M_{VEHICLE} * (V_{MAX})^2 / R_{BEND} = 2224.07 \text{ N} \quad (5)$$

The above loading acts upon the instantaneous apex and bottom section of the hub creating a torque loading condition over the Side length of the Hub.

The Hub may face impact from another Vehicle or from a fence or any other obstacle. Taking the upper loading Possibility of 2G force due to side impact,

$$F_{SIDE\ IMPACT} = 2 * 9.8 * 300 \text{ N} = 5886 \text{ N} \quad (6),$$

On the outer face of the hub resulting in load of 1471.5N on each Petal.

The Final Load to be added is the Torsional Moment on the Spindle, which over-looked a lot of times but for large number of cycles and Lightweight vehicles with highly uneven terrain of operation, affects the fatigue dynamics a lot.

$$T_{TORSION} = M_{VEHICLE} * f_{REAR} / 2 * 9.8 * R_{WHEEL} * = 191.394 \text{ N} \quad (7)$$

The above 7 equations thus give all possible significant loads on the hub of an all-terrain vehicles with appropriate assumptions. The following loads will be applied accordingly for the simulation phase of the design process. The Brake Torque is applied on the rotor mount in the direction opposite to the forward motion of the vehicle. The Bump force is applied on the Hub leaves giving fixed spindle as fixed constraint. The cornering torque is applied as moment on the plane parallel to the ground on the laterally extreme leaves. The torsion on spindle is simulated keeping the leaves and rotor mounts fixed and finally the bump force is again done keeping the spindle fixed and applied on the leaves [5] [6].

Design

The design has been prepared on Solid works initially and then modified after topology optimization using Ansys Spaceclaim and Topology Optimization tool after constraining mass to at least 55% the original value. The Final Design is as follows:

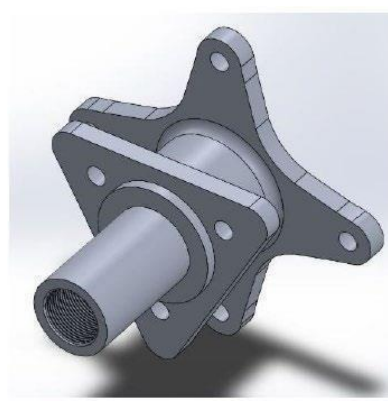

Figure 2. Design of Integrated Hub-Stub Component

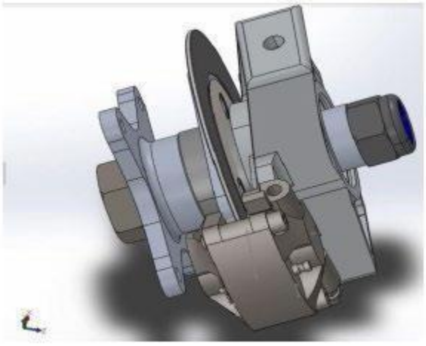

Figure 3. Design of Integrated Hub-Stub Component

Design Failure and Mode Analysis (DFMEA)

DFMEA is a tool commonly used in analyzing the structural safety of any component. It comprises of four main factors:

1. Risk Priority Number (RPN): Represents the overall risk associated with the component. Higher the risk, Higher the RPN.
2. Severity (S): It is the measure of how severely the failure of a component might affect the vehicle and the driver. Higher the Severity, Higher the S rating.
3. Occurrence (O): This is the measure of how frequently the component failure occurs in a general automobile. Higher the Occurrence chances, higher the O rating.
4. Detection (D): It represents the measure of how easily the failure of the particular component is detected. Failures more difficult to detect receive a higher D rating

The factors are interrelated by the following relation:

$$RPN = S * O * D \quad (8)$$

Standard Severity, Occurrence and Detection Charts as specified by Society of Automotive Engineers (SAE) have been followed for the wheel assembly [15] [16]. Adding to that we have also discussed about what can be the remedial actions to prevent failure, to be kept in mind while doing simulations and analysis. Possible testing measures can be stress testing using a Universal Testing machine and multiple Lap tests before actually rolling out on road or in races. Discussion of these physical testing procedures is not under the scope of this paper. [18]

Table 1. DFMEA Table for standard ATV Wheel Assembly

COMPONENT	SEVERITY (S)	OCCURRENCE (O)	DETECTION (D)	RISK PRIORITY NUMBER (RPN)
TIRES	7	6	2	84
RIMS	8	3	4	96
KNUCKLES AND HUBS	8	4	5	160

Table 1 highlights the fact that Hubs are the components with the highest risk factor associated. This necessitates a high Factor of Safety (FOS) to be kept while designing the component. Thus the topology optimization study conducted had the second Criteria to ensure a Minimum FOS of 2 under Static Conditions. No constraint was applied to the Dynamic Case as we went for analysis of the Extreme case of all 7 loads acting at once which is an extremely rare scenario.

Simulation and Analysis

ANSYS was the tool of choice for our simulations. We covered three main tools for our analysis, Static Structural, Fatigue Analysis for the dynamic case, and, Topology Optimization Tool for Mass optimization subject to Mass retention of 55% and Static FOS of 2. Spaceclaim was then used for cleaning out geometry and making necessary changes for a machinable product [17]. The Final Results from the topology Optimization run has been shown in Figure 4.

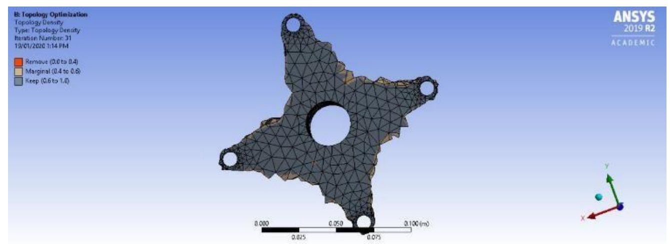

Figure 4. Topology Optimization before Spaceclaim post processing

Proper Mesh refinement techniques were employed at the edges and transitions to capture accurate results at the places where loads were high from the preliminary initial uniform meshing analysis as shown in Figure 5, part a and b. This practice of local meshing improves the speed of results without affecting Convergence.

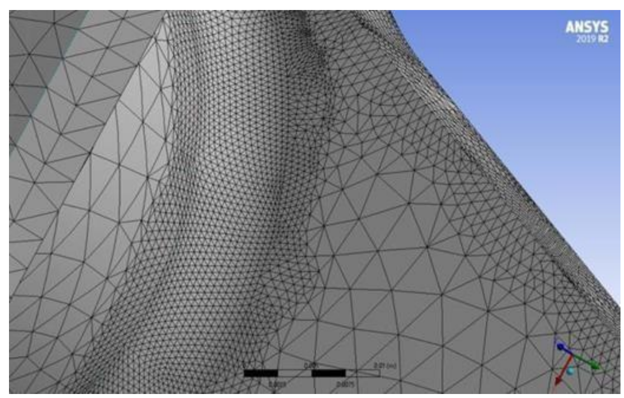

Figure 5 (a). Local Mesh Refinements

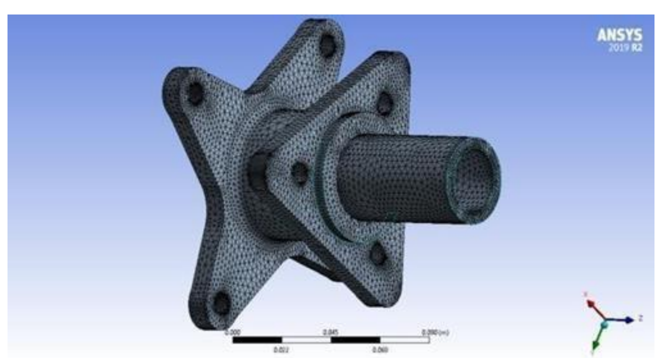

Figure 5 (b). Global Mesh on the integrated design

Figure 6 and 7 show Deformation and Factor of safety from a Static run, where all loads were applied at once. This is an extreme case which is highly unlikely to occur but has been chosen to give a good margin on Factor of Safety for standard loading conditions.

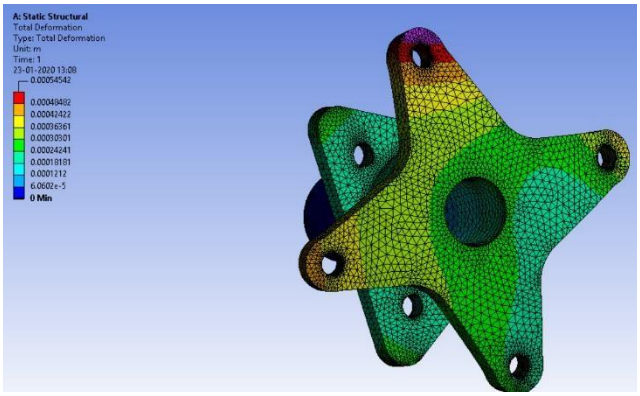

Figure 6. Deformation Contours over the integrated design

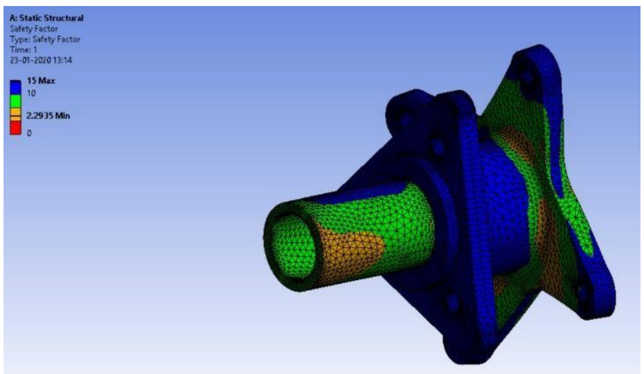

Figure 7. Factor of Safety Contours over the integrated design

The Fatigue analysis was done using Stress Life Theory and taking the Goodman theory of failure analysis, based on fully reversed Loading Scenario. For calculation of maximum stress amplitude for achieving the target lifetime of operation of a component, the stress life approach is followed. For target life of greater than 1000 cycles, this approach is found to be much more standard and appropriate. The theory is based upon stress vs. cycles of life curve also called the S-N curve. The kind of pattern associated to loading in our component is found to be alternating tensile and compressive stresses also referred as fully reversed loading as shown in Figure 8. [3][4]

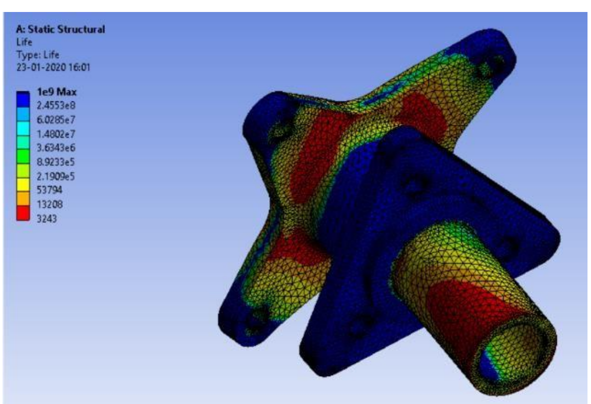

Figure 8. Life in No. of Cycles, as a contour mapped over the Surface

Figure 9 shows the fatigue sensitivity of the dynamic simulation case. The above results were simulated for the most extreme of the cases taking all the above forces acting on the unibody all at the same time. The actual scenario is a lot different and at most 60-75% load acts on the vehicle at any given time. The fatigue sensitivity plot thus shows the number of cycles of operations at various fractions of load, ranging from 50%, which is mostly the realistic smooth drive scenario, to 150%, representing extreme crash cases or highly rocky terrain with continuous bump and side impact on the wheels. Thus, we can realistically expect around 7000-9000 cycles of operations terrains such as a BAJA track and around 11000 cycles of operations on a general graveled road.

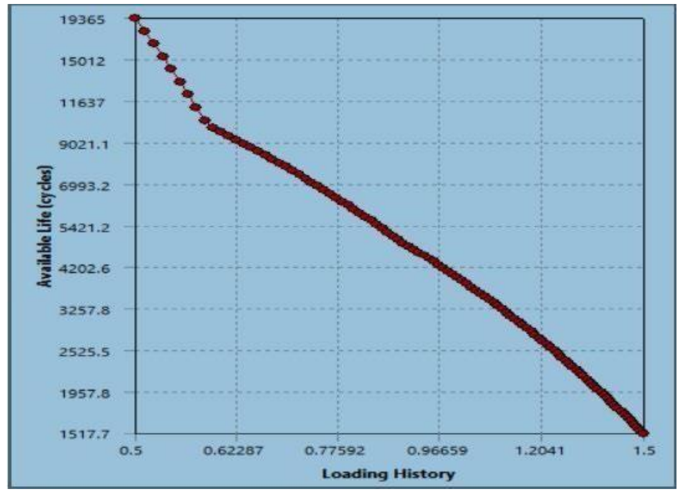

Figure 9. Fatigue Sensitivity Plot

The material properties associated with fatigue analysis are generally uniaxial in nature. But for real life applications stress states are usually multi-axial. The Biaxiality parameter thus gives some idea of the stress states over the model and gives better interpretation of the results. Biaxial indication can be understood as the ratio of the principal stress having lesser magnitude over the greater principal stress ignoring near zero principal stresses. A value of zero signifies uniaxial stress, while a value of -1 denotes pure shear, the value of 1 denotes a state of pure bi-axiality. The FOS contour figure can be interpreted along with the biaxial contour, with maximum stress regions developing mostly at places predominantly under uniaxial stress states. The advantage of this study would be that, if it is observed that maximum deformation is obtained at a region of pure shear, it is better to utilize S-N experimental data obtained using torsional loading conditions. In the current scenario, collecting experimental data for various loading conditions is quite costly and mostly done only for academic study or by large manufacturers. The results from the biaxial study are shown in Figure 10. To aid a close comparative analysis the Dynamic FOS contour has been given together with the biaxial results in Figure 11. As is evident from a comparative view point with FOS showing a strong spatial correlation with uniaxial stress states as suggested in theory, validating the accuracy of the loading conditions and numerical simulation. We shall later analyse the stability of our Boundary conditions through a convergence study on majorly three parameters, Life Cycles under maximum loading to prove the stability of the numerical scheme under Dynamic Loading, Factor of Safety in the cases of statically load boundary conditions, and, maximum deformation under static conditions. All the parameters will be plotted against mesh defeaturing size. [5][6]

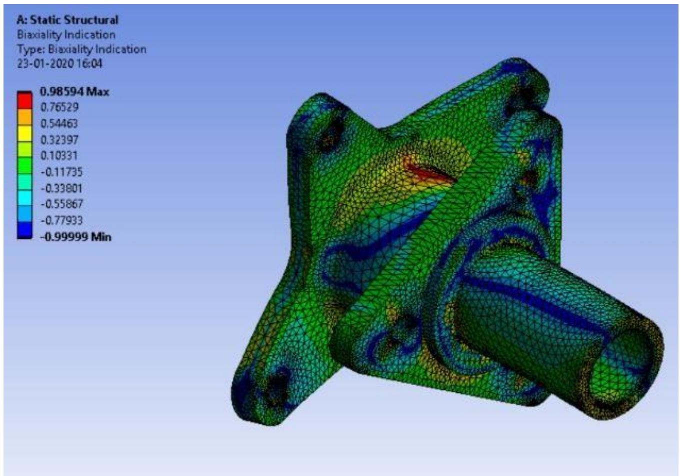

Figure 10. Biaxiality Indication parameter contour mapped over the surface

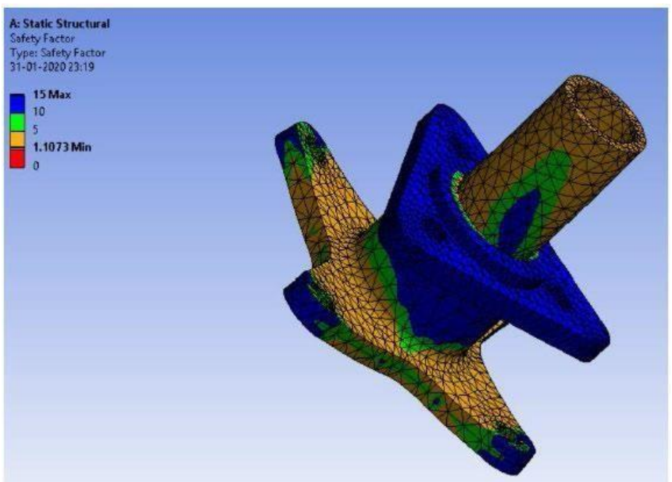

Figure 11. Factor of Safety from Dynamic Test Run (100% Loading)

Analysis of the dimensional convergence of a computer based numerical simulation is a prevalent method for analyzing the accuracy of the error associated with the ordered discretization/meshing. The method involves an iterative process of running consecutive simulations decreasing the grid size or resolution. Upon continuous refining as the elements become smaller in size and their quantity in the flow domain in-crease also as the time step is diminished, the errors associated with temporal and dimensional discretization should approach zero asymptotically, obviously excluding some numerical errors. Analysis methods for evaluating the pre-mentioned convergence criteria are mentioned by Roache in his book. The methods arise out of the standard

Richardson techniques of extrapolation. We wanted to go for Finite

Volume Method for Convergence as it is more sensitive to Divergence than the Finite Element Method. A high-density fluid should be selected for the flow domain, preferably water, instead of air for tightness in measure for convergence calculations. We used the SST K-omega model as it offers better operation and execution for flows over wall-boundary layers involving a characteristically low Reynolds number and free shear. [7]

The graphs in this section show how the results change as we vary the element size in an iterative manner. Convergence is achieved when the solution changes by a magnitude of ε. ε, is often termed as correction scalar or termination scalar in convex optimization or simulation processes. It is defined as the desired norm between 2 successive iterations. Hence it can also be described as error factor. For general realistic simulation procedures ε is taken as .00000001. Hence, Convergence is achieved when the norm between two scalars reaches the ε value mentioned above. An important consideration before proceeding with the analysis is that the bounding box setup for the Boolean subtract operation should be extended longer at the outlet face to properly capture fluid flow and improve the accuracy. The Inlet was kept at 7L from the leading face, 8L each from the top and bottom walls and the outlet was kept at 15L from the trailing edge of the geometry. This ensures that there is no domain dependence of the convergence calculations. The results are shown in Figure 12, 13 and 14.

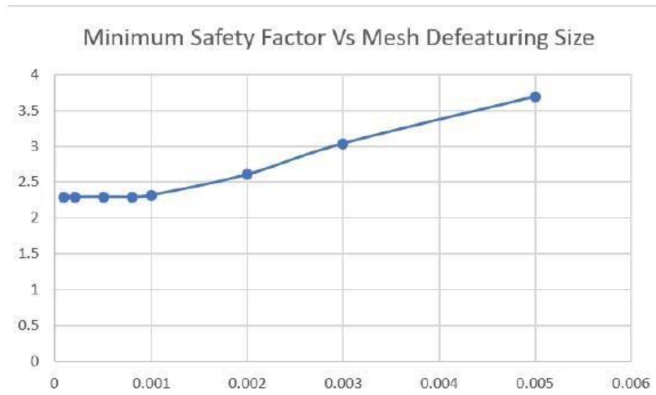

Figure 12. Factor of Safety Convergence Study

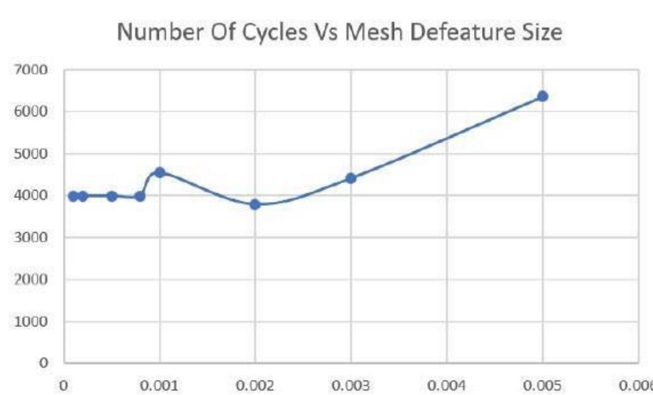

Figure 13. Dynamic Conditions Convergence Study

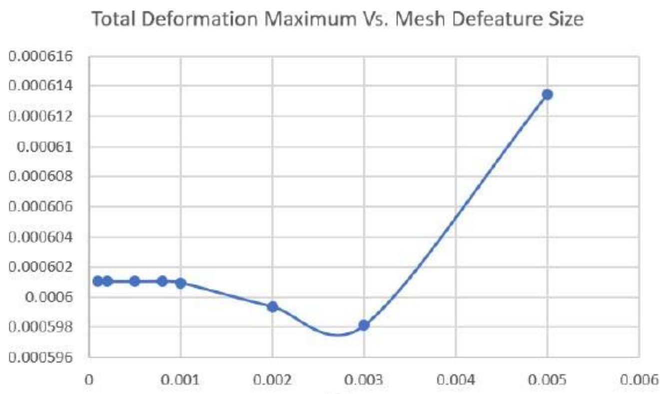

Figure 14. Static Study Deformation Results Convergence Study

The Data from the Convergence study is tabulated in Table 2 for visualization and clarity. It can be clearly observed that we start achieving convergence from fifth iteration onwards. Full convergence took 8 iterations to complete.

Iteration	Mesh Defeature Size (in Meters)	Mesh Nodes	Mesh Elements	Total Deformation	FOS	Minimum Life
1	.005	6033	3191	.000613474	3.692138	6352.302961
2	.003	12929	7097	.000598136	3.036720	4404.013688
3	.002	17082	9431	.000599382	2.604572	3779.147928
4	.001	21748	11864	.000600969	2.314553	4539.93864
5	.0008	26750	14738	.000601049	2.935629	3986.218007
6	.0005	26750	14738	.000601049	2.935638	3986.218007
7	.0002	26750	14738	.000601049	2.935428	3986.218007
8	.0001`	26750	14738	.000601049	2.935428	3986.218007

The major data found from the simulation run have been summarized in Table 3 for clarity. The results show acceptable values for similar class of vehicles from various related studies. [18][19][20]

Table 3. Summary of Key Values obtained from Simulation cases (After Convergence)

RESULT	Maximum Value	Minimum Value	Average Value
Deformation	.6 mm	.2 mm	NA
Von Mises Stress	135 MPa	1854.4 Pa	19.7 MPa
Von Mises Strain	.0019617	$4.963*10^{-8}$	.000299
Factor of Safety (FOS)	15	2.29	12.58
Life (No. of Cycles)	NA	3986	NA
Dynamic FOS	15	1.1073	9.7627
Biaxiality Indication	.98594	-.9999	-.18756

The key takeaways from the above data not discussed earlier are the values of Von Mises Stress and Von Mises Strain. Both have been calculated for the static case. A dynamic analysis for the same was not done as it does not contribute to understating and analyzing the design since a 100% loading scenario rarely occurs in practice. For the static case the maximum obtained Von Mises Stress comes out to be 135 MPa. Chosen Alloy Al 6061-T6 has an Ultimate Tensile Strength of 42 ksi, or, 290 MPa. It also has a Yield strength of at least 240 MPa. Both of these value are well clear of the obtained Von Mises Stress. The contour obtained for Von Mises Stress under Static Loading is shown in Figure 15.

Analyzing the dimensionless Von Mises Strain parameter, we obtain a pretty safe and standard maximum value of around .002 (m/m). Given the average value over the contour of around .0003 (m/m), it will be safe to say that we don't encounter major deformation dependency over the geometry. Nonetheless, the contour for Equivalent or Von Mises Strain has been shown in Figure 16.

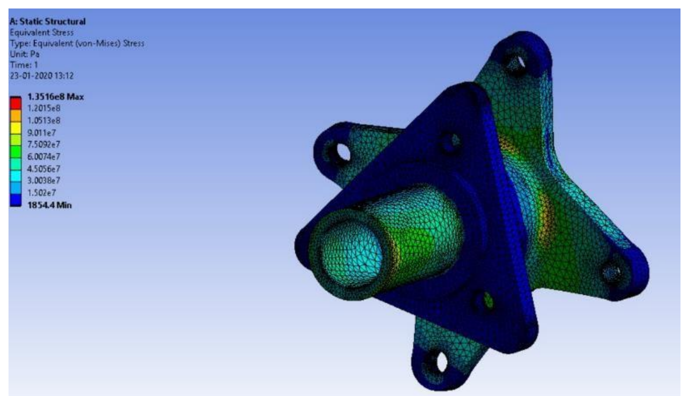

Figure 15. Static Von Mises Stress Contour mapped over the surface

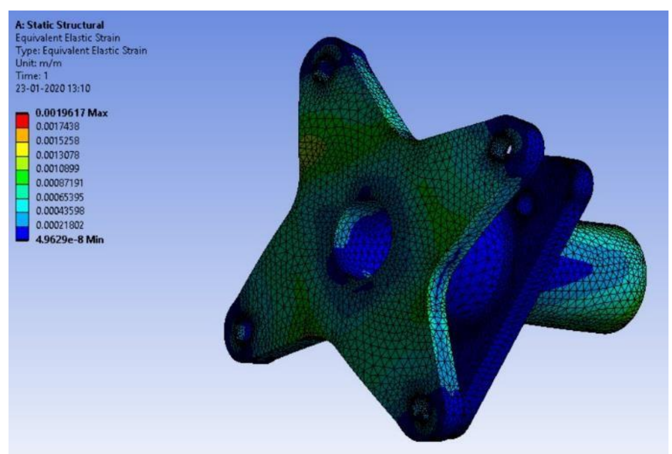

Figure 16. Static Von Mises Strain Contour mapped over the surface

Conclusion

We have successfully designed and analyzed a model for the integrated stub- Wheel Hub component. The Minimum FOS is maintained at a very good and safe ratio of 2.29 and max deflection is .6 mm. The Hub Mass and thus the unsprung mass has been reduced by 25.55%. This is a significant development from the existing design. This directly improves Vehicle speeds and driver comfort by reducing vibrations due to the unsprung weight, which in turn increases driver confidence and handling going into corners. Thus, this improvement also increases a vehicle's cornering performance indirectly. Techniques such as mesh refinement, Topology Optimization, Grid Independence and Stress Life Theory have been adopted for analysis and simulations. DFMEA has been adopted as a check against the possible Risk of failure of the Component and analyzing the best methods to reduce the risk.

We have done a check using 3 material and found that Al 6061-T6 is the best compromise on comparison with Al 7475 T6 and EN8. We have considered every possible force and loading actions on the components based on extensive literature survey cross checking. The max shear stress developed is $1.35*10^8$ Pa and max elastic strain is $1.9*10^{-3}$ m/m. For fatigue life analysis we have used Goodman criteria and Soderberg criteria due to which results of the number of cycles after which body fails is 3986 and 3239 respectively. Also, we have used topology optimization to get the finer design with lesser mass. Finally, we have fulfilled our aim of manufacturing a modified wheel hub design which does not affect any other components of the ATV.

References

1. Kaya, Necmettin & Karen, Idris & Öztürk, Ferruh. (2010). Redesign of a failed clutch fork using topology and shape optimisation by the response surface method. Materials & Design - MATER DESIGN. 31. 3008-3014. 10.1016/j.matdes, doi: 2010.01.002.
2. S.Dhar "Fracture analysis of wheel hub fabricated from pressure die aluminium assembly theoretical and applied fracture mechanics" , vol 9 feb 1988,pp 5-11
3. Nitin S Gokhale, Sanjay S Deshpande, Sanjeev V Bedekar, Anand N Thite, January 2008, Practical finite element analysis (Pune: Finite to Infinite), First edition
4. Bader, Qasim & Njim, Emad. (2014). Mean stress correction effects on the fatigue life behavior of steel alloys by using stress life approach theories.. International Journal of Emerging Technologies in Learning (iJET). 14 (4).
5. Preeti Vishwakarma, Mukesh Kanungoo, February 2014, Finite element analysis of Chevrolet front hub with the help of inventor, IJITE, Vol-02, Issue-02, p 11, 12.
6. S. M. A. Kazimi. (1982). Solid Mechanics. Tata McGraw-Hill. ISBN 0-07-451715-5
7. Roache, P.J., K. Ghia, and F. White, "Editorial Policy Statement on the Control of Numerical Accuracy," ASME Journal of Fluids Engineering, Vol. 108, No. 1., March 1986, p. 2, doi: 10.1115/1.3242537
8. Mr. Mohammad Raffi, Mr. Ganapa Raghu Vamsi Reddy, Mr. U. Yashvanth, 2019, Structural Analysis of a ATV Wheel Hub, INTERNATIONAL JOURNAL OF ENGINEERING RESEARCH & TECHNOLOGY (IJERT) Volume 08, Issue 03 (March – 2019)
9. Poojari, Mohan & Kamarthi, Ashwin & Shetty, Kshitij & Sanil, Adithya & Palan, Karthik. (2019). DESIGN AND ANALYSIS OF THE WHEEL HUB FOR AN ALL- TERRAIN VEHICLE WITH THE PLASTIC POLYMER: NYLON- 6,6. Journal of Mechanical Engineering Research & Developments. 42. 119-123, doi: 10.26480/jmerd.05.2019.119.123.
10. Saxena, Gaurav & Chauhan, Ankit & Jain, Rohit & Gupta, Ishwar. (2017). Simulation and Optimization of wheel Hub and Upright of Vehicle: A Review. IOSR Journal of Mechanical and Civil Engineering. 14. 42-50, doi: 10.9790/1684-1401034250.
11. Kumar, Rajan & Bharj, Rabinder. (2020). Design and Development of the Front Wheel Hub for All-Terrain Vehicle (ATV). Journal of Mechanical Engineering. 17. 49-62.
12. García, J.. "Analysis of Wheel Hubs : Student Car." (2014).
13. M.Ravi Shankar, Srinivasan Chandrasekar, W.Dale Compton, Alexander H. King, Characteristics of aluminum 6061-T6 deformed to large plastic strains by machining, Materials Science and Engineering: A, Volumes 410–411, 2005, Pages 364-368, ISSN 0921-5093, doi: 10.1016/j.msea.2005.08.137.
14. Ohnistova, Petra; Piska, Miroslav; Petrenec, Martin; Dluhos, Jiri; Hornikova, Jana; Sandera, Pavel. 2019. "Fatigue Life of 7475-T7351 Aluminum After Local Severe Plastic Deformation Caused by Machining" *Materials* 12, no. 21: 3605, doi: 10.3390/ma12213605
15. Jawagar Shrehari J, Raagul Srinivasan K A, "Failure Modes and Effective Analysis of All-Terrain Vehicle and Go-Kart: A Review", International Journal of Science and Research (IJSR), https://www.ijsr.net/search_index_results_paperid.php?id=ART20163722, Volume 5 Issue 12, December 2016, 1543 – 1547
16. Biček, Matej & Gotovac, Gorazd & Miljavec, Damijan & Zupan, Samo. (2015). Mechanical Failure Mode Causes of In-Wheel Motors. Strojniški vestnik - Journal of Mechanical Engineering. 61. 74-85, doi: 10.5545/sv-jme.2014.2022.
17. Chang Yong Song, Jongsoo Lee, Reliability-based design optimization of knuckle component using conservative method of moving least squares meta-models, Probabilistic Engineering Mechanics, Volume 26, Issue 2, 2011, Pages 364-379, ISSN 0266-8920, doi: 10.1016/j.probengmech.2010.09.004.
18. Fischer, G. and Grubisic, V., "Design Criteria and Durability Approval of Wheel Hubs," SAE Technical Paper 982840, 1998, doi: 10.4271/982840.
19. Shukla, Pranjal & Joshi, Konark & Rastogi, Utkarsh & Moola, Ajith. (2019). Design Analysis and Simulations of Components of an All-Terrain Vehicle, doi: 10.4271/2019-28-0049.
20. Peshin, C., Walia, M., Madhan, P., and Gaikwad, S., "Design and Simulation of Components of an All-Terrain Vehicle," SAE Technical Paper 2020-28-0486, 2020, doi: 10.4271/2020-28-0486

Contact Information

1. Urooj Ahmad; B.E. Mechanical Engineering, E-Mail: f20180652@hyderabad.bits-pilani.ac.in https://www.linkedin.com/in/uroojahmad

2. Subhrat Praharaj; B.E. Mechanical Engineering, M.Sc. Mathematics E-Mail: f20180714@hyderabad.bits-pilani.ac.in https://www.linkedin.com/in/subhrat-praharaj-485666193

Acknowledgments

We would like to thank our SAE Baja Team, Team Vulcan, for their constant support as this paper draws upon the knowledge of various subsystems and where this prototype was implemented for the competitions. We would also like to thank our HOD Dr. N. Suresh Kumar Reddy who is also the Faculty in charge of Team Vulcan along with Dr. Sandip S. Deshmukh. Finally, we would like to thank Dr. R. Parameshwaran, Dr. Y.V.D Rao and Dr. R Sujith for taking time out of their busy schedules and suggesting improvements in presentation of the contents of this paper.

Definitions/Abbreviations

Symbol	Physical Quantity
c_m	Cost Per unit Mass
F_{STEP}	Stepping Force on Pedal
F_{MC}	Force on Master Cylinder
F_{PISTON}	Force on each Piston
$D_{PISTON, C}$	Diameter of piston in the calliper
$D_{PISTON, MC}$	Diameter of Cylinder
$T_{BRAKING}$	Braking To
μ_{PAD}	Coefficient Brake Pad a
N_{PISTON}	Number of
D_{RIM}	Diameter of
f_{REAR}	Fraction of
V_{MAX}	Maximum
$M_{VEHICLE}$	Mass of Ve driver
F_{BUMP}	Bump Force
$F_{CORNERING}$	Cornering Force
R_{BEND}	Radius of Bend
$F_{SIDE\ IMPACT}$	Side Impact Force
$T_{TORSION}$	Torsional Moment
R_{WHEEL}	Wheel Radius

Appendix

The following figures are additional images regarding the entire Wheel Carrier assembly and Design Iterations Drawings of the Integrated Wheel Hub-Stub Axle Component. These have been attached so as to give the reader an insight to designing the carrier assembly corresponding to the integrated design.

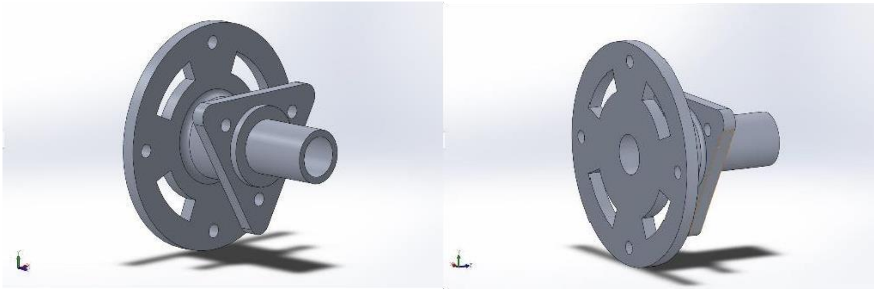

Figure 17. Front and Rear Views of the Initial Design

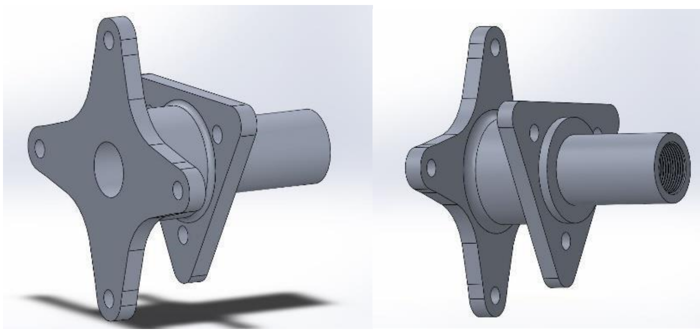

Figure 18. Front and Rear Views of the Final Design after Topology Optimization

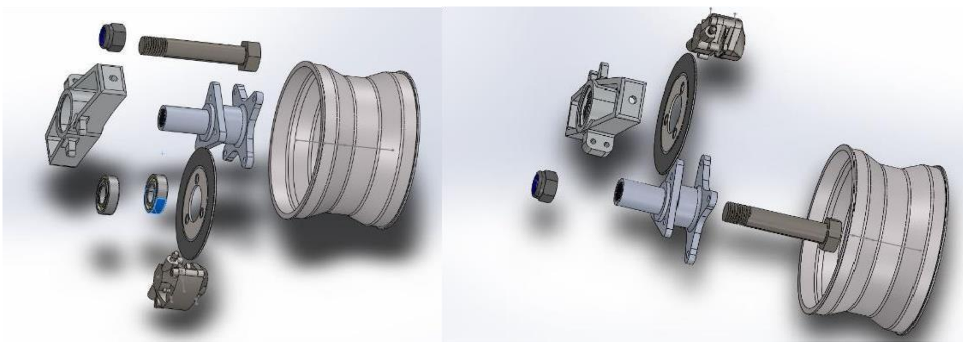

Figure 19. Exploded View of Wheel Carrier Assembly

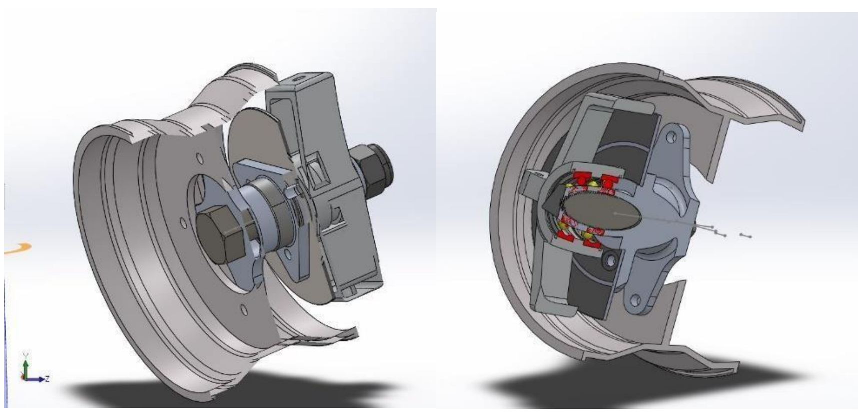

Figure 20. Cross Section View of Wheel Carrier Assembly showing positioning of Bearings and Rotor Disc